Fiber Mach-Zehnder Interferometer system using polymer optical Bragg grating for underwater applications

Carlos A. F. Marques[1,2], David J. Webb[2]

[1]Instituto de Telecomunicações and Physics Department & I3N, Universidade de Aveiro, Campus de Santiago, 3810-193 Aveiro, Portugal
[2]Aston Institute of Photonic Technologies, Aston University, Aston Triangle, B4 7ET Birmingham, UK
*Corresponding author: cmarques@av.it.pt

Abstract: In the subsea environment, the monitoring of acoustic signals and vibration is crucial for different applications such as in geophysical surveying and security, e.g. the detection of unwanted craft or personnel. Current technology is predominantly based on piezoelectric (PZT) strain sensors but they suffer from some limitations. To solve these problems, fiber Bragg grating (FBG) sensors are considered as potential alternatives for conventional PZT hydrophones. In this paper, we present our recent experimental studies on FBG based acoustic sensing using polymer optical fiber (POF) in a comparison with the response of silica fiber. Fiber Mach-Zehnder interferometers (MZI) are widely used for FBG sensor interrogation purpose due to their advantages in terms of high resolution, wide bandwidth, and tunable sensitivity. They are appropriate for dynamic strain measurement applications in the areas of vibration analysis, hydrophones, and acoustic emission studies. The interferometer converts the Bragg wavelength shift of an FBG sensor into a corresponding phase shift in an electrical carrier, which can be demodulated using conventional techniques.
In this paper, an interferometric scheme for monitoring low-frequency (few kHz) waves using silica and polymer FBGs is investigated. A heterodyne technique based on an unbalanced interferometric wavelength discriminator is described and the performance of both types of fiber containing FBGs is compared. A considerable sensitivity improvement is achieved using polymer FBG (around 6 times better), and we could explain that considering the lower Young's modulus of POF. Essentially, and despite the strain sensitivity of silica and POFBGs being very similar, this renders the POF much more sensitive to the applied stress resulting from acoustic signals. Results give noise-limited pressure resolutions of 3.68×10^{-6} and 1.33×10^{-4} Pa for silica and POF, respectively, each within a 100 Hz bandwidth.

1. Introduction

Optical fibre based sensors are transforming industry by permitting monitoring in hitherto inaccessible environments or measurement approaches that cannot be reproduced using conventional electronic sensors. A multitude of techniques have been developed to render the fibres sensitive to a wide range of parameters including: temperature, strain, pressure (static and dynamic), acceleration, rotation, gas type, and specific biochemical species [1-3]. Constructed entirely of glass or polymer material [1-4], optical fibre devices like fibre gratings offer a number of attractive features: low loss (especially for silica fiber), dielectric construction, small size, multiplexing capability, and so on [1-3]. In recent years, fiber Bragg grating (FBG) sensors have generated great interests because of their versatile applications in in-situ strain, temperature and pressure monitoring, among others [1-9]. Besides the general advantages of fiber optic sensors, FBG sensors provide many additional attractive features over competing technologies and hence are enjoying widespread acceptance.
The monitoring of acoustic signals and vibration in the subsea environment is crucial for different applications such as in geophysical surveying and security (detection of unwanted craft or personnel). Current technology is predominantly based on piezoelectric strain sensors. They have satisfactory performance but suffer from other limitations: physical size; limited deployment range without local power and amplification (contributing further to physical size); lack of multiplexing capabilities. To solve these problems, there has been a steady move to introduce optical fibre based systems, firstly for surveillance [10] and for geophysical surveying [11]. The first such systems were interferometric in nature, involving coils of fibre wound on a compliant mandrel. Such systems still have the disadvantage of requiring a large diameter cable to contain the coil. Efforts have been made to use Bragg grating sensors along a single straight fibre, but for the most demanding applications standard Bragg gratings do not possess sufficient sensitivity and it has proven necessary to use fibre laser sensors [12], which although keeping the sensor diameter down, add to complexity and cost. Recently, optical hydrophones [13] offer a means of overcoming these difficulties. Previous fibre sensor research has focussed on silica fibres

and only now, with the increasing maturity of the polymer FBG technology have the first relevant but preliminary studies been carried out, looking at an accelerometer, assessing strain response up to a few kHz [14] and demonstrating a fibre grating based acoustic modulator [7]. Very recently, a fiber Mach-Zehnder interferometer (MZI) based silica FBG sensor was reported for underwater low-frequency sensing [15,16]. In this paper, an interferometric scheme for monitoring low-frequency (few kHz) waves using silica and polymer FBGs is investigated. A heterodyne technique based on an unbalanced interferometric wavelength discriminator is described and the performance of both types of fiber containing FBGs is compared. A considerable sensitivity improvement is achieved using polymer FBG (around 6 times better), which arises as a result of the much more compliant nature of POF compared to silica fiber (3 GPa vs 72 GPa, respectively). Essentially, and despite the strain sensitivity of silica and POFBGs being very similar, this renders the POF much more sensitive to the applied stress resulting from acoustic signals or vibration. Preliminary results give noise-limited pressure resolutions of 3.68×10^{-6} and 1.33×10^{-4} Pa for silica and polymer optical fiber (POF), respectively, each within a 1 Hz bandwidth.

2. Experiment

The arrangement used to interrogate the grating is shown in Fig. 1. This utilized a ramped lithium niobate phase modulator (accurately set to produce a 2π peak-to-peak phase excursion) to frequency shift the light in one arm of an unbalanced MZI and thus allowed the use of heterodyne signal processing [17,18]. Light from a broadband light source (provided by Thorlabs ASE-FL7002-C4), giving an output power of 20 mW centered at 1560 nm with a bandwidth of 80 nm, was launched into the unbalanced MZI; hence a channelled spectrum was created at the interferometer's outputs that was incident on the grating. Incorporated in one arm of the MZI was the phase modulator. The other arm contained a variable air gap that allowed the optical path difference (OPD) between the two arms to be adjusted. Provided that the OPD between the MZI's arms is longer than the source coherence length and shorter than the effective coherence length of the back-reflected light from the grating, interference signals are observed at the detector, which can be expressed as

$$I(\lambda_B) = A\left\{1 + V\cos\left[\omega_r t + \Phi + \delta\Phi\sin\omega t + \phi(t)\right]\right\}, \quad (1)$$

where λ_B is the wavelength of the reflected light from the modulated grating, ω_r is the angular frequency of the ramp modulation, ω is the angular strain frequency experienced by the grating, A is proportional to the grating reflectivity, V is the visibility of the signals, $\Phi = 2\pi OPD/\lambda_B$, where $OPD = n_{eff}\delta L$, and $\Phi(t)$ is a random phase-drift term. A sinusoidal strain-induced change in λ_B from the FBG, ($\delta\lambda_B$), induces a change in phase shift in Eq. (1), given by

$$\delta\Phi\sin\omega t = \left(2\pi OPD/\lambda_B\right)\left(\delta\lambda_B\right)\sin\omega t \quad (2)$$

Hence from Eq. (1) strain-induced changes in λ_B induce a corresponding phase modulation of the electrical carrier produced at the detector by the phase modulator, which we measured by determining the amplitudes of the upper and lower sideband frequency components observed on an FFT spectrum analyser.

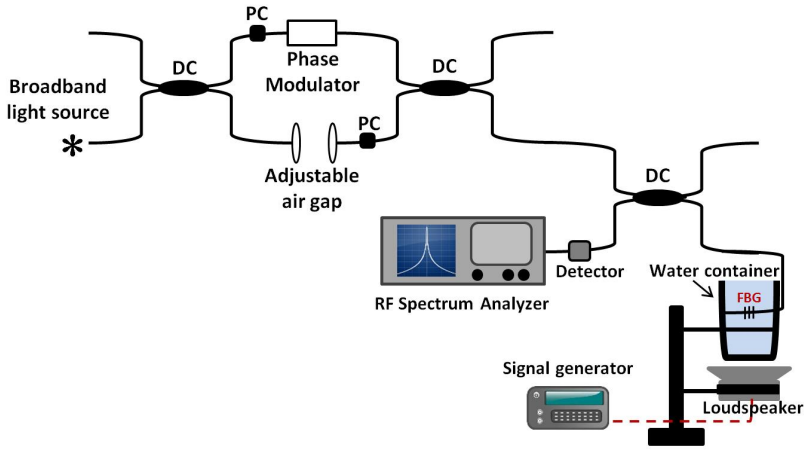

Figure 1. Experimental arrangement. DC: directional coupler, PC: polarization controller.

Two effects affect the sensitivity of the system. First, from Eq. (2), an increase in OPD results in a proportional increase in the amplitude of the phase modulation. Second, increasing the OPD beyond the coherence length of the light reflected by the FBG results in a reduction in the visibility and consequently the height of the carrier and sidebands. Therefore, the sensitivity was optimized by adjusting the OPD to achieve the maximum sideband amplitude. Initially, we calculated the OPD between the two arms of the designed MZI be recording the interference pattern on an OSA using the broadband source. Then, the length difference δL between the two arms of the MZI can be calculated by

$$\delta L = \frac{\lambda_B^2}{2\pi n_{eff}\delta\lambda_B}\delta\phi\,, \tag{3}$$

where $\delta\phi$ is the phase difference, and $\delta\phi=2\pi$ for two adjacent peaks separated by the free spectral range.

3. Sensitivity and Results

When the fibre is compressed, the fractional change $\delta\lambda_B/\lambda_B$, induced in the Bragg wavelength λ_B, in response to a pressure change δP, is given by [19]

$$\frac{\delta\lambda_B}{\lambda_B} = \frac{\Delta\left(n_{eff}\Lambda\right)}{n_{eff}\Lambda} = \left[\frac{1}{\Lambda}\frac{\partial\Lambda}{\partial P} + \frac{1}{n_{eff}}\frac{\partial n_{eff}}{\partial P}\right]\delta P\,, \tag{4}$$

where Λ is the spatial period of the grating. The fractional change in physical length of the fiber and refractive index of the fiber core, respectively, are given by

$$\frac{\delta L}{L} = -\frac{(1-2\upsilon)P}{E} \tag{5}$$

$$\frac{\delta n_{eff}}{n_{eff}} = \frac{n_{eff}^2 P}{2E}(1-2\upsilon)(2p_{12}+p_{11}) \tag{6}$$

where E and υ are the Young modulus and Poisson ratio of the fiber, respectively, and p_{11} and p_{12} are the components of the strain-optic tensor. As the fractional change in the spatial period of the grating equals the fractional change in the physical length of the sensing section, the pressure sensitivity is then expected to be [19]

$$\frac{1}{\lambda_B}\frac{\delta\lambda_B}{\delta P} = -\frac{1}{E}\left((1-2\upsilon) - \frac{n_{eff}^2}{2}(1-2\upsilon)(2p_{12}+p_{11})\right) \quad (7)$$

With reference to equation (7), the first part in the parenthesis relates to the change in the period of the fabricated grating planes within the fibre core, whereas the second part relates to the refractive index change as a result of the strain optic effect. However, equation (7) is relevant for an isotropic solid, which is acceptable for silica optical fibre; conversely POF is not an isotropic material and so equation (7) may lack validity for POF. During the drawing process of POF manufacture the molecular polymer chains tend to align along the fibre axis, and are therefore an example of a transverse isotropic material where the properties perpendicular to the fibre axis are not the same as the properties that are along the fibre axis.

Using the values presented in Table 1 for the parameters E, υ, n_{eff}, p_{11} and p_{12} for silica and polymer fibers, the predicted fractional wavelength shift is -2.8x10^{-6} /MPa using silica fiber and -1.8x10^{-6} /MPa using polymer fiber, an improvement around 1.5 times for homogenous PMMA fiber. In fact, from [20] the measured fractional changes were -2.5x10^{-6} /MPa (for silica fiber) and 83x10^{-6} /MPa (for POF), where these experimental results refer to some initial static pressure tests, and they showed that the wavelength shift with POF is opposite to that with silica (and much higher in magnitude). We could only explain that by allowing the fibre to be anisotropic as mentioned above.

From our experimental results and using the Bessel Function, the $V_{sideband}/V_{carrier}$ for POF and silica were 0.35 and 0.06, respectively, which means $V_{sideband}/V_{carrier} = J_1(phase)/ J_0(phase)$ where $J_0\ (phase)$ is approximately 1 for small phase modulations [21,22]. So, after calculating the $J1\ (phase)$ for both cases, we achieved $J_1(phase)$ 0.17 for POF case, and 0.025 for silica fiber. With this signal processing scheme, the phase modulation we measured is directly proportional to the wavelength modulation experienced by the FBG. In fact, the amplitude of the wavelength modulation is given by $\lambda_B^2\Phi / 2\pi OPD$. So, the wavelength modulation for the POF is about 6 times greater than that for the silica. The significant difference between our results when compared with work in [20] can be explained by our fiber perhaps being less anisotropic; typically, the case if the fiber is drawn under lower stress.

Table 1: Material properties of PMMA and fused silica.

	PMMA	**Fused silica**
Parameter		
p_{11}	0.300	0.126
p_{12}	0.297	0.26
E (GPa)	2.95	72.45
n_{eff}	1.481	1.465
υ	0.37	0.165

The phase modulator was ramped, and hence generated a carrier signal, at 10 kHz. The silica and polymer FBGs had nominal Bragg wavelengths of 1550.21 nm and 1573.42 nm, with reflectivities of 90% and 80%, respectively, and both FBGs had a bandwidth around 0.5 nm. Hence, in this scheme, acoustically induced changes in the wavelength reflected from FBG induce a phase modulation of the electrical carrier produced by the phase modulator, which we measured by determining the amplitudes of the side bands observed on the spectrum analyser. As shown in Fig. 1, a standard 8 Ω loudspeaker was driven in continuous mode by a signal generator tuned at the frequency 420 Hz to excite the FBG in water (and in air for comparison). Acoustic signals coming from the loudspeaker excites vibrations in the container, where the FBG is attached, which in turn, induces strain in the FBG sensor.

Fig. 2 (a) shows the 10 kHz carrier signal and sidebands observed on the spectrum analyzer for 0.0625 and 25 W of acoustical power from the loudspeaker when the silica FBG is in air. Fig. 2 (b) shows the detected power of the sidebands (normalized with respect to the carrier signal power) as a function of the acoustical power. From Fig. 2 (b), the results demonstrate a highly linear response over the entire measurement region. The same analysis, but using the container with water, is shown in Figs. 3 (a) and (b). In this case, the difference between carrier amplitude and sidebands amplitude is reduced (25 dB) when compared with the case in air (29 dB). The signal-to-noise ratio measured by the spectrum analyser was 52 dB. Therefore, if the noise-limited resolution is

defined as the RMS pressure amplitude that would lead to a signal-to-noise ratio of unity, the resolution may be calculated to be 3.68×10^{-5} Pa within a 100 Hz bandwidth, corresponding to 3.68×10^{-6} Pa/Hz$^{1/2}$.

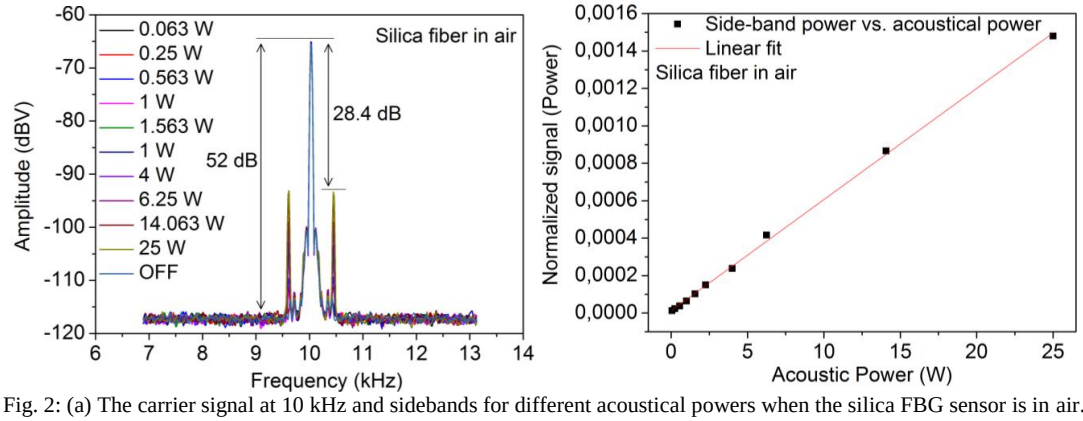

Fig. 2: (a) The carrier signal at 10 kHz and sidebands for different acoustical powers when the silica FBG sensor is in air. (b) The side-band power (normalized with respect to the carrier power) as a function of the acoustical power.

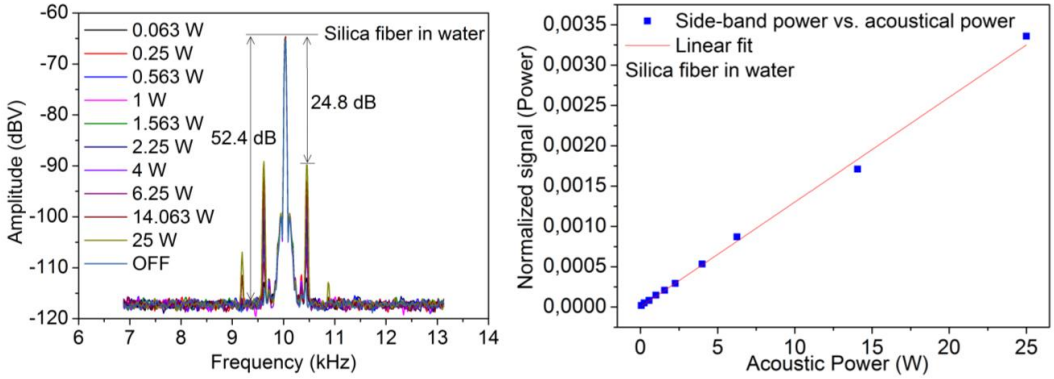

Fig. 3: (a) The carrier signal at 10 kHz and sidebands for different acoustical powers when the silica FBG sensor is in water. (b) The side-band power (normalized with respect to the carrier power) as a function of the acoustical power.

Tests were conducted when a POFBG is used instead of silica FBG. The previous conditions presented for silica FBG are kept to compare the performance. Fig. 4 shows the 10 kHz carrier signal and sidebands observed on the spectrum analyzer for no power from loudspeaker and for 25 W of acoustical when the POFBG is in air. In air, we can observe that the sidebands amplitude is weak at 25 W of acoustical power when compared with silica FBG sensor case. Fig. 5 (a) presents the carrier signal at 10 kHz and sidebands for acoustical power from 0.0625 to 25 W, when the container has the POFBG in water. Fig. 5 (b) illustrates the detected power of the sidebands (normalized with respect to the carrier signal power) as a function of the acoustical power. Here, the sidebands are strong compared with the air case, showing a high linear response. The difference between carrier and sidebands amplitude is reduced when compared with the case of a silica FBG sensor, achieving 9 dB of difference, almost 3 times less than the silica FBG sensor in water. The signal-to-noise ratio measured by the spectrum analyser was 17 dB. To determine the noise-limited resolution of the system, the same procedure was used as above and it was 1.33×10^{-4} Pa/Hz$^{1/2}$.

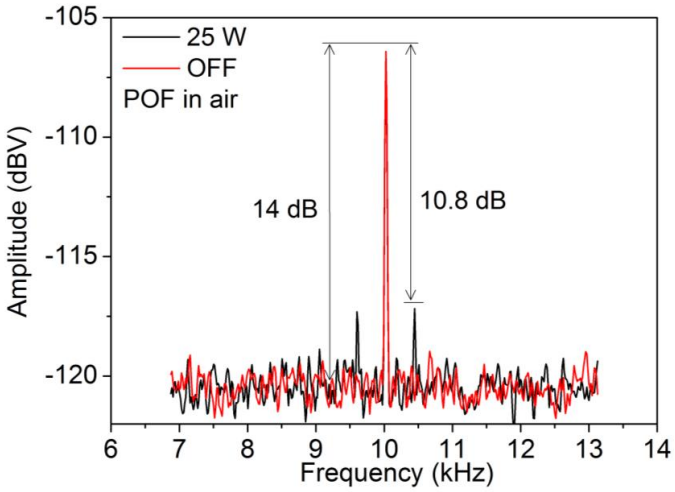

Fig. 4: The carrier signal at 10 kHz and side bands for acoustical powers at 0 W (OFF) and 25 W when the POFBG sensor is in air.

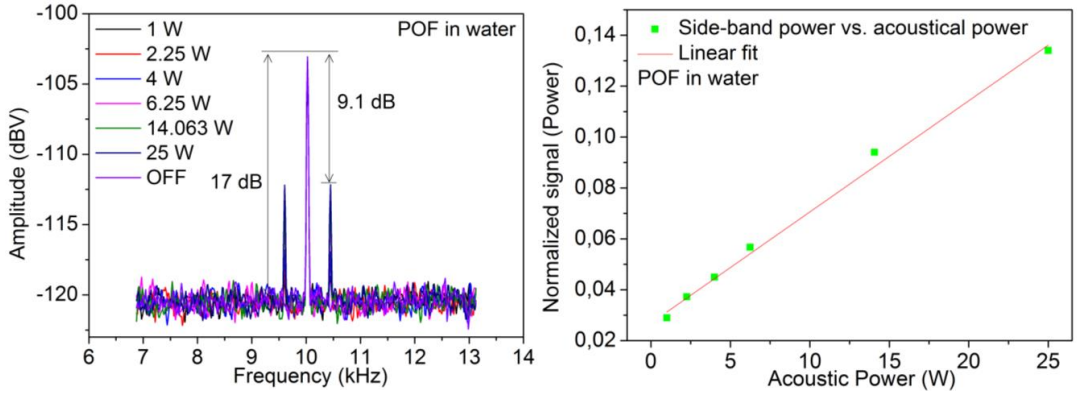

Fig. 5: (a) The carrier signal at 10 kHz and side bands for different acoustical powers when the POFBG sensor is in water. (b) The side-band power (normalized with respect to the carrier power) as a function of the acoustical power.

4. Conclusions

In conclusion, we have presented our recent experimental results towards the development of a polymer FBG based sensor for underwater acoustic sensing. A FBG based sensor head and a fiber MZI interferometer has been fabricated for this purpose for monitoring low-frequency (few kHz) waves. A heterodyne technique based on an unbalanced interferometric wavelength discriminator is described and the performance of both types of fiber containing FBGs is compared. A considerable sensitivity improvement is achieved using polymer FBG (around 6 times better), which arises as a result of the much more compliant nature of POF compared to silica fiber. These results give us noise-limited pressure resolutions of 3.68×10^{-6} and 1.33×10^{-4} Pa for silica and POF, respectively.

5. Acknowledgments

This work was supported by Marie Curie Intra European Fellowship included in the 7th Framework Program of the European Union (project PIEF-GA-2013-628604). Also, C. Marques is grateful for the FCT Fellowship SFRH/BPD/109458/2015.

6. References

[1] T. G. Giallorenzi, J. Bucaro, A. Dandridge, G. Sigel, J. Cole, S. Rashleigh, R. Priest, "Optical fiber sensor technology," IEEE Trans. Microw. Theory Techn. 30, 472 (1982).

[2] S. Yin, P. B. Ruffin, F. T. S. Yu, Fiber Optic Sensors, 2nd ed. Boca Raton, FL, USA: CRC Press, 2008.

[3] A. Othonos, K. Kalli, Fiber Bragg Gratings: Fundamentals and Applications in Telecommunications and Sensing. Norwood, MA, USA: Artech House, (1999).

[4] D. J. Webb, "Fiber Bragg grating sensors in polymer optical fibers," Meas. Sci. Technol. 26, 092004 (2015).

[5] H. B. Liu, H. Y. Liu, G. D. Peng, P. L. Chu, "Strain and temperature sensor using a combination of polymer and silica fibre Bragg gratings," Opt. Commun. 219, 139 (2003).

[6] K. Peters, "Polymer optical fiber sensors - A review," Smart Mater. Struct. 20, 013002 (2011).

[7] C. A. F. Marques, L. Bilro, L. Kahn, R. A. Oliveira, D. J. Webb, R. N. Nogueira, "Acousto-Optic effect in microstructured polymer fiber Bragg gratings: simulation and experimental overview", IEEE/OSA J. Lightw. Technol. 31, 1551 (2013).

[8] C. A. F. Marques, G. D. Peng, D. J. Webb, "Highly sensitive liquid level monitoring system utilizing polymer fiber Bragg gratings," Opt. Express 23, 6058 (2015).

[9] N. J. Alberto, C. A. F. Marques, J. L. Pinto, R. N. Nogueira, "Three-parameter optical fiber sensor based on a tilted fiber Bragg grating," Appl. Opt. 49, 6085 (2010).

[10] G. A. Cranch, R. Crickmore, C. K. Kirkendall, A. Bautista, K. Daley, S. Motley, J. Salzano, J. Latchem, P. J. Nash, "Acoustic performance of a large-aperture, seabed, fiber-optic hydrophone array", Journal of the Acoustical Society of America 115, 2848 (2004).

[11] P. J. Nash, G. A. Cranch, D. J. Hill, "Large scale multiplexed fibre-optic arrays for geophysical applications", Proceedings of the Society of Photo-Optical Instrumentation Engineers (SPIE) 42022000, 55 (2000).

[12] G. A. Cranch, G. A. Miller, C. K. Kirkendall, "Fiber laser sensors: Enabling the next generation of miniaturized, wideband marine sensors", Proceedings of Fiber Optic Sensors and Applications VIII (SPIE) 8028 (2011).

[13] M. Moccia, M. Consales, A. Iadicicco, M. Pisco, A. Cutolo, V. Galdi, A. Cusano, "Resonant Hydrophones Based on Coated Fiber Bragg Gratings," IEEE/OSA J. Lightwave Technol. 30, 2472 (2012).

[14] A. Stefani, S. Andresen, W. Yuan, O. Bang, "Dynamic Characterization of Polymer Optical Fibers", IEEE J. Sensors 12, 3047 (2012).

[15] B. Das, A. P. Narayan, U. Tiwari, "Fiber Bragg Grating based Acoustic Sensing with Interferometric Interrogation," in 12th International Conference on Fiber Optics and Photonics, M4A.17 (2014).

[16] V. Chandra, U. Tiwari, B. Das, "Elimination of Light Intensity Noise Using Dual-Channel Scheme for Fiber MZI-Based FBG Sensor Interrogation," IEEE Sensors Journal 16, 2431 (2016).

[17] D. A. Jackson, A. D. Kersey, M. Corke, J. D. C. Jones, "Pseudo-heterodyne detection scheme for optical interferometer", Electron. Lett. 18**,** 1081 (1982).

[18] N. E. Fisher, D. J. Webb, C. N. Pannell, D. A. Jackson, L. R. Gavrilov, J. W. Hand, L. Zhang, I. Bennion, "Ultrasonic hydrophone based on short in-fiber Bragg gratings," Appl. Opt. 37, 8120 (1998).

[19] M. G. Xu, L. Reekie, Y. T. Chow, J. P. Dakin, "Optical in-fibre grating high pressure sensor," Electronics Letters 29, 398 (1993).

[20] Ian P. Johnson, David J. Webb, Kyriacos Kalli, "Hydrostatic pressure sensing using a polymer optical fibre Bragg gratings", Proc. of SPIE Vol. 8351 - 3rd Asia Pacific Optical Sensors Conference, 835106 (2012).

[21] https://www.st-andrews.ac.uk/~www_pa/Scots_Guide/RadCom/part12/page1.html

[22] http://uspas.fnal.gov/materials/08UCSC/mml16_modulation_and_detection.pdf